

A nanoscale combing technique for the large-scale assembly of highly aligned nanowires

Jun Yao¹, Hao Yan¹ and Charles M. Lieber^{1,2,*}

The controlled assembly of nanowires is a key challenge in the development of a range of bottom-up devices^{1,2}. Recent advances^{2–19} in the post-growth assembly of nanowires and carbon nanotubes have led to alignment ratios of 80–95% for a misalignment angle of $\pm 5^\circ$ (refs 5,12–14) and allowed various multiwire devices to be fabricated^{6,10–13,19}. However, these methods still create a significant number of crossing defects, which restricts the development of device arrays and circuits based on single nanowires/nanotubes. Here, we show that a nanocombing assembly technique, in which nanowires are anchored to defined areas of a surface and then drawn out over chemically distinct regions of the surface, can yield arrays with greater than 98.5% of the nanowires aligned to within $\pm 1^\circ$ of the combing direction. The arrays have a crossing defect density of ~ 0.04 nanowires per μm and efficient end registration at the anchoring/combing interface. With this technique, arrays of single-nanowire devices are tiled over chips and shown to have reproducible electronic properties. We also show that nanocombing can be used for laterally deterministic assembly, to align ultralong (millimetre-scale) nanowires to within $\pm 1^\circ$ and to assemble suspended and crossed nanowire arrays.

Nanowires can be assembled in solution using electric or magnetic fields^{3,4,7}, fluid flows^{5,6}, the Langmuir–Blodgett technique^{8–10} and bubble-blown films¹⁴, but creating high-density individually connected nanowire arrays in an efficient and scalable manner remains challenging. Mechanical printing¹⁶ overcomes a number of these problems and has been used to make multi-nanowire and multi-nanotube devices, including circuitry for artificial skin²⁰ and integrated circuits on plastic substrates²¹. However, the alignment ratios obtained with this approach (~ 90 – 95% at a $\pm 5^\circ$ misalignment angle^{12,13}) can still lead to crossing defects that limit the application of printing for single-nanowire devices.

We hypothesized that the alignment limitations in previous work were due to the fact that forces used to anchor and align nanowires coexist in the same substrate (printing) regions; that is, the anchoring force necessary for the attachment of nanowires to the device substrate can oppose the aligning force and result in less effective orientational control. Hence, improvements in the alignment of nanowires during assembly might be achieved by separating the anchoring location of nanowires from the aligning region, an approach termed nanocombing in analogy to combing/straightening of hair anchored to the scalp or the molecular combing reported previously for DNA²².

There are several essential features of the nanocombing process (Fig. 1a). First, separate anchoring regions with strong nanowire interactions and aligning regions with weaker nanowire interactions are lithographically patterned on the target substrate. Second, the nanowire growth substrate is brought into contact with the target substrate and translated in the desired direction with a defined

applied force and speed. During contact and translation, the protruding nanowire ends first stick to the anchoring surface, then the remaining length is pulled over the combing surface, where the aligning force, which is diametrically opposed to the anchoring force, is maximized due to the weak interaction with the combing surface.

We first demonstrate the essential feature of the nanocombing technique by transferring silicon nanowires²³. We used a functionalized SiO_2 surface and a resist-layer surface as the anchoring and combing surfaces, respectively. The target substrate was patterned with an organic resist layer (Microposit S1805) where the exposed SiO_2 regions, which were modified with tetramethylammonium ions during pattern development, served to improve the anchoring of silicon nanowires to the exposed SiO_2 regions during transfer (see Methods). The combing process was then carried out by sliding the nanowire growth substrate over the target substrate at a constant velocity and pressure, with high-viscosity hydrocarbon liquid added between the two surfaces.

Scanning electron microscopy (SEM) images of the silicon nanowire arrays obtained from nanocombing onto a substrate with an array of anchoring regions (Fig. 1b–d) reveal several important points. First, for constant $15\text{-}\mu\text{m}$ -length anchoring regions the nanowires show excellent alignment in the combing regions over lengths varying from 15 to $80\text{ }\mu\text{m}$ and a total single array length of $500\text{ }\mu\text{m}$. Qualitatively, the SEM images show extremely straight and parallel nanowires regardless of position within the array shown in Fig. 1b. Second, this high degree of nanowire alignment was observed over macroscopic dimensions in the nanocombing process; that is, nanocombed nanowires in 40 arrays over a $3\text{ mm} \times 11\text{ mm}$ area of a substrate chip (Supplementary Fig. S1) exhibit alignment similar to that in Fig. 1b–d. Third, comparison of the nanowires in the anchoring and combing regions (Supplementary Fig. S2) clearly shows the lower alignment, higher crossing defects and slightly higher nanowire density in the anchoring region. All three observations are consistent with our model for nanocombing and previous studies^{12,13}. Fourth, the upper portion of Fig. 1b, where the length of the combing region (dark) is $80\text{ }\mu\text{m}$ (versus $15\text{ }\mu\text{m}$ for the anchoring region), shows nanowires are only present starting from and closer to the anchoring region (direction of combing is upward in the image), and are largely absent from the remainder of the combing region. These observations highlight the stronger interaction of the anchoring region acting to trap nanowires versus the weak interaction between the nanowires and the combing surface.

Quantitative analysis of alignment determined from analysis of more than 1,600 nanowires from arrays over the substrate chip (Fig. 1e) showed that $\sim 98.6\%$ of the combed nanowires are aligned to within $\pm 1^\circ$ of the combing direction, representing better than tenfold improvement in alignment compared with previous reports^{5,12–14,18} (see Methods). Moreover, the high degree of alignment

¹Department of Chemistry and Chemical Biology, Harvard University, Cambridge, Massachusetts 02138, USA, ²School of Engineering and Applied Science, Harvard University, Cambridge, Massachusetts 02138, USA. *e-mail: cml@cmliris.harvard.edu

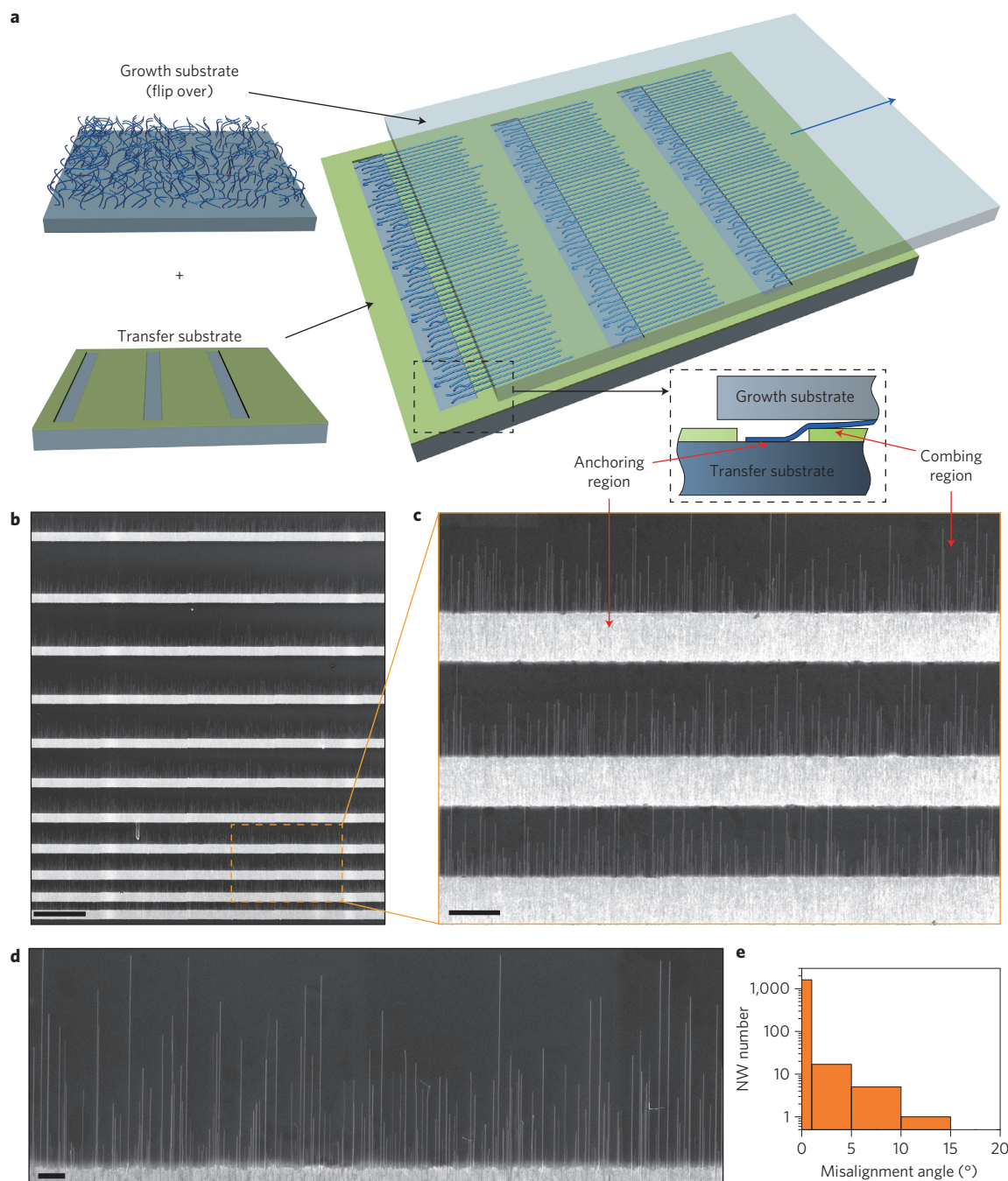


Figure 1 | Schematics and demonstration of nanocombing. **a**, Schematics of the nanocombing process. The blue arrow indicates the travelling direction of the growth substrate with respect to the target substrate, which yields a combing/aligning force that is parallel and opposite to the anchoring force. The dashed window at the right bottom shows a side view of the nanocombing process. **b–d**, SEM images of silicon nanowires on the combing (resist) surface at different magnifications. The thickness of the resist (S1805) layer was ~ 70 nm. Scale bars: $50\ \mu\text{m}$ (**b**), $10\ \mu\text{m}$ (**c**), $2\ \mu\text{m}$ (**d**). **e**, Angle distribution of the combed nanowires obtained from analysis of nanowire arrays combed over a $3\ \text{mm} \times 11\ \text{mm}$ chip, where the logarithm of nanowire (NW) number is plotted with respect to misalignment angle (see Methods for details).

results in a low crossing defect density, ~ 0.04 nanowire per μm (see Methods), which is also tenfold better than values achieved at similar nanowire densities by contact printing¹⁸. Importantly and as will be discussed further in the following, the highly aligned and low crossing defect density allows for the fabrication of high yields of reproducible individual nanowire devices.

We also explored several directions to determine key factors controlling nanowire density, as well as factors important to the nanocombing process. We first investigated how the length of the anchoring region affects nanowire density in the combing region.

A summary of nanowire density as a function of length of anchoring region (Fig. 2a) shows that the density increases and then saturates at ~ 1.5 nanowires per μm as the anchoring length increases from 2 to $15\ \mu\text{m}$; no further density increases were observed as the anchoring length was increased to $30\ \mu\text{m}$. Interestingly, the average nanowire length in the combing region (Supplementary Fig. S3) is only weakly dependent on anchoring length. Our analysis shows that, for an average as-grown length of $\sim 30\ \mu\text{m}$, the average combing length is $\sim 7\ \mu\text{m}$ (Supplementary Fig. S3). Considering the $\sim 50\%$ reduction in nanowire length resulting from breakage by friction

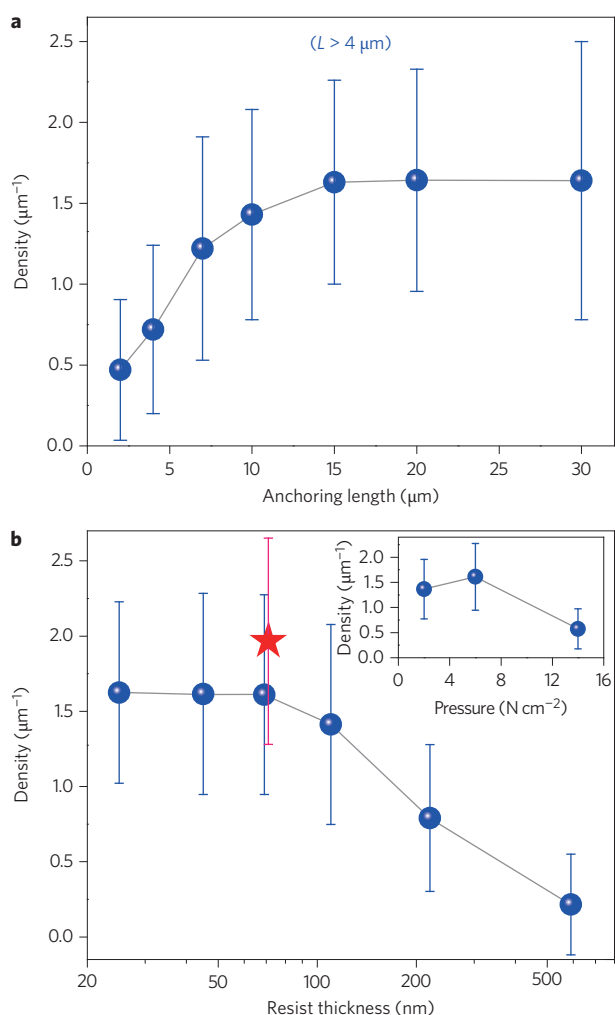


Figure 2 | Nanowire density control. **a**, Silicon nanowire density on the combing (resist) surface with respect to different anchoring lengths. The statistics are based on nanowires with lengths $>4 \mu\text{m}$. Data are from the sample shown in Fig. 1b–d. **b**, Nanowire density with respect to different resist/combing layer thicknesses. The anchoring surfaces were modified using the same conditions in all cases. The star indicates the combed nanowire density by anchoring-surface modification using 10 s development and 50 s KOH treatment. Inset: nanowire density with respect to different combing pressures. The nanowire density comparisons in **b** are all based on the same anchoring length of $30 \mu\text{m}$.

reported previously¹³, this yields an estimated ratio of $\sim 1:1$ between anchoring length and combing length. Furthermore, we note that the apparent density decrease for anchoring lengths $\leq 10 \mu\text{m}$ (Fig. 2a) shows the critical role of the anchoring region in trapping nanowires during the nanocombing process. We also find that much longer nanowires yield a corresponding increase in aligned, nanocombed length (discussed in the following).

Second, investigations of the nanowire density versus resist thickness (Fig. 2b) show that the combing density is approximately constant up to a value of $\sim 70 \text{ nm}$, and decreases with increasing resist thickness above this value. This result is consistent with the nanocombing model (Fig. 1a), as an increased separation of the growth surface reduces the efficiency of nanowire contact with and trapping by the anchoring surface region. Below this value, the combing density is largely independent of resist thickness. Moreover, studies of nanowire density as a function of contact pressure (Fig. 2b, inset) show that the density is largely independent of pressure between ~ 2 and 6 N cm^{-2} , which provides a relatively

broad window for nanocombing. At higher contact pressures, above $\sim 10 \text{ N cm}^{-2}$, we observe a decrease in density, which shows that simply forcing the two surfaces together cannot yield an increased number of nanowires per unit area. Additional studies are needed to define the origin of the decreased density at higher pressures (for example, enhanced fragmentation of nanowires on the growth substrate and/or anchoring region), but the density-independent range of pressures is indicative that surface interactions within the anchoring region are dominant.

Third, we have carried out several experiments to better illuminate factors important to the nanocombing process. When the patterned SiO_2 surface is developed for a minimum amount of time (8 s versus 50 s) and then more extensively rinsed with deionized water (30 s versus 10 s) to minimize the effect of tetramethylammonium hydroxide in the developer, we find a much lower nanowire density (0.3 nanowires per μm), using the optimum anchoring length and overall resist thickness discussed previously. Furthermore, when the developed SiO_2 surface of the anchoring regions is rinsed with dilute potassium KOH solution (50 s, $\sim 1.5 \text{ wt\% KOH}$), we observe a further increase in the combing density to almost 2 nanowires per μm (Fig. 2b, star). Contact angle measurements (Supplementary Fig. S4) further show that higher densities can be associated with the more hydrophilic anchoring region, and also confirm that the combing regions are hydrophobic. Moreover, measurements carried out using a mineral oil/octane mixture as well as isopropyl alcohol as the transfer liquid (Supplementary Fig. S5) suggest that the liquid polarity, but not viscosity, is most important in enhancing the density and alignment of nanowires in nanocombing. These studies suggest that further increases in density may be achieved through variations in the anchoring-surface chemistry²⁴. Finally, experiments carried out with nanocombing rate varied by a factor of ten (Supplementary Fig. S6) show that the density and alignment ratio are approximately independent of the combing speed, thus suggesting that following attachment in the anchoring region the necessary/required alignment force is lower than the minimum shear value accessed (consistent with a weak nanowire-combing surface interaction).

The highly aligned nanowires produced over large areas by nanocombing open up the potential to fabricate hierarchical arrays of single-nanowire devices. Compared with previously reported assembly methods^{5,6,8–14}, which generally lack end-to-end registration⁹ for individual nanowires, nanocombing ensures that the aligned nanowires in an array start from the anchoring/combing interface patterned by lithography. Hence, registration of one end can be readily controlled in arrays patterned on a substrate, as shown in Fig. 3a,b. With the ‘start’ of nanowires in the arrays defined by nanocombing, it is then straightforward to define a uniform ‘end’ edge by lithography-based trimming to yield well-aligned and uniform-length nanowire arrays over the substrate surface (Fig. 3c, Supplementary Fig. S7). Obtaining uniform-length nanowires in every array using this approach places constraints on this length, because there are variations in the nanowire length from the anchoring/combing interface (Fig. 1), as already discussed. Despite this limitation, we can readily obtain well-aligned and uniform nanowire arrays with lengths of $2\text{--}5 \mu\text{m}$, and the average combing length can be increased by increasing the length of nanowires on the growth substrate. To estimate the device density for applications (Supplementary Information, ‘Nanowire density analysis’), an alternating pattern of $10 \mu\text{m}$ anchoring and combing lengths with $4 \mu\text{m}$ resultant trimmed nanowire length yields 20% nanowire surface coverage and a device density of $7 \times 10^6 \text{ cm}^{-2}$. This could be increased to 27% nanowire surface coverage and a device density of $1 \times 10^7 \text{ cm}^{-2}$ if a less conservative combing length of $5 \mu\text{m}$ were used. In either case, the device density values are $10\text{--}100\times$ higher than that achieved previously^{15,17}.

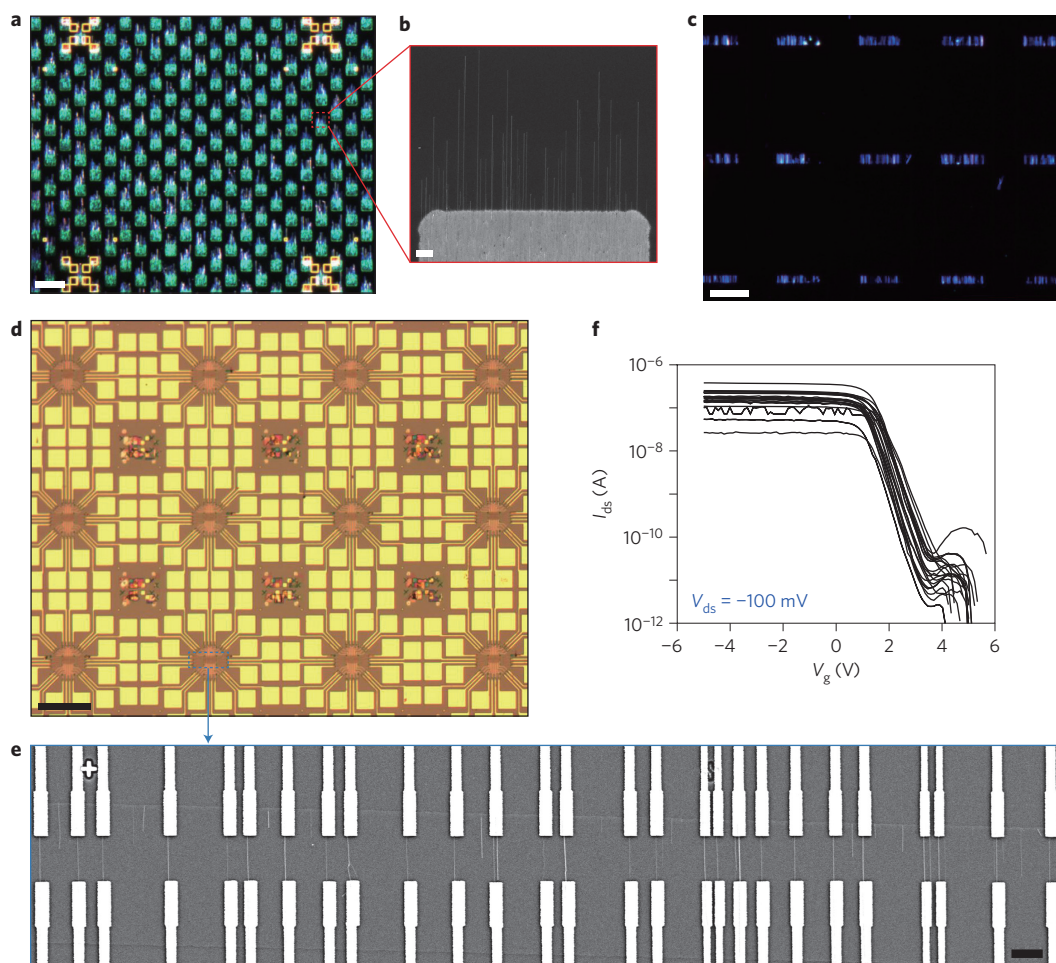


Figure 3 | Nanowire device arrays. **a**, Dark-field image of silicon nanowire arrays. The anchoring windows were defined by photolithography, and the resist layer (S1805) thickness was ~ 70 nm. Scale bar, 100 μm . **b**, SEM image of one of the combed nanowire arrays on the resist layer. Scale bar, 2 μm . **c**, Dark-field image of trimmed nanowire arrays (resist layer removed). Scale bar, 40 μm . **d**, Optical image of nanowire device arrays connecting to electrode arrays. Scale bar, 200 μm . **e**, Representative SEM image of one of the device arrays. Scale bar, 2 μm . **f**, $I_{\text{ds}}-V_{\text{g}}$ characteristics ($V_{\text{ds}} = 0.1$ V) from 20 top-gated Ge/Si nanowire devices assembled by nanocombing. The channel length of the devices is ~ 3.8 μm , with Al_2O_3 (7 nm) serving as the dielectric layer for the top gate (Cr/Au = 5/50 nm). The electrical characterizations were performed in an ambient environment.

As an example of the fabrication of device arrays, patterned, trimmed nanowire blocks were used to fabricate arrays of single-nanowire field-effect transistors (FETs). Photolithography was used to define a periodic array of electrodes around each block of aligned nanowires (Fig. 3d). The individual nanowires were then connected using electron-beam lithography. SEM images (Fig. 3e) demonstrate the high yield of individual nanowire devices for each block, which is readily achieved due to the excellent nanowire alignment and end-to-end registration. In other words, the trimming step, which is registered to the anchoring/combing interface, makes the fabrication nearly deterministic with respect to the y -coordinate (where y is defined as the nanowire axis). The typical yields of single-nanowire FETs achieved by this approach are $\sim 90\%$, and exceed the $\sim 60\%$ achieved in our recent work using direct printing²⁵. We also applied nanocombing to assemble Ge/Si core-shell nanowire arrays so as to directly compare the reproducibility of FET properties with previous work. Current versus gate-voltage data from 20 representative devices (Fig. 3f) show that the individual nanowire FETs have reproducible behaviour. Of particular importance to the development of integrated circuits is the threshold voltage, which has an average ± 1 s.d. (standard deviation) of 1.7 ± 0.2 V, where the variation in threshold is substantially better than that reported recently for Ge/Si nanowire

devices assembled by direct contact printing²⁵ (1.2 ± 0.7 V). Moreover, the scaled ON current of $0.40 \text{ mA } \mu\text{m}^{-1}$ (scaled channel length of 1 μm) is similar to that reported for single high-performance Ge/Si nanowire devices²⁶ without consideration of arrays. We note that the variation of ON current (Fig. 3f) is similar to that seen in isolated nanowire devices, and probably results from variations in contact resistance and individual nanowire properties²³. Taken together, these results indicate that the nanocombing process preserves the critical electrical transport properties of nanowire devices.

We have also explored the potential of extending nanocombing to laterally deterministic assembly (and an overall nearly deterministic fabrication process) by defining the x -coordinates of nanowires during nanocombing. Conceptually, laterally deterministic assembly can be enabled by controlling the widths of the anchoring windows (Fig. 4a, left) such that narrow, periodic anchoring windows produce a periodic or other predetermined pitch nanowire array. A representative SEM image of the silicon nanowire array produced by this method (Fig. 4a, right) shows that a majority of the anchoring windows yield single, highly aligned nanocombed silicon nanowires. Significantly, individual nanowire devices can then be fabricated without registration to the nanowires, because the pattern of contact electrodes simply matches the original

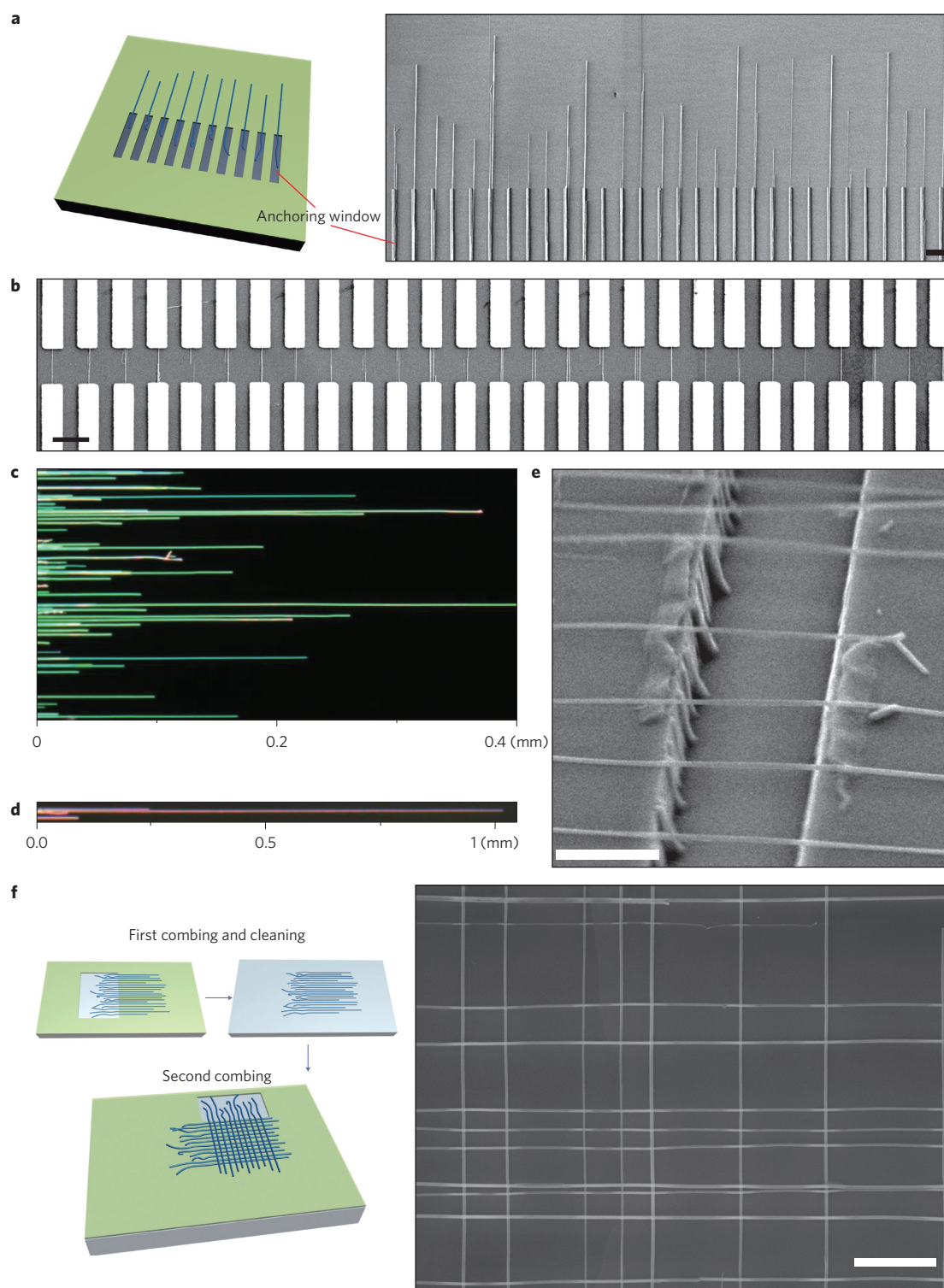


Figure 4 | Nanocombing applications. **a**, Left: schematic of periodic silicon nanowire array by nanocombing. Right: SEM image of the resulting periodic nanowire array on the resist (PMMA) surface. Each anchoring window has a $300 \text{ nm} \times 15 \text{ } \mu\text{m}$ ($W \times L$) SiO_2 surface defined by electron-beam lithography, with the PMMA layer (thickness of $\sim 50 \text{ nm}$) serving as the combing surface. The SiO_2 surface was functionalized in MF-319 (50 s) and cleaned (20 s in deionized water) before combing. Scale bar, $2 \text{ } \mu\text{m}$. **b**, SEM image of a periodic silicon nanowire device array made from the combing method shown in **a**. **c**, Dark-field image of ultralong silicon nanowires on the combing surface (70 nm S1805). **d**, A millimetre-long combed silicon nanowire on the resist surface. **e**, SEM image of a suspended silicon nanowire array. The resist layer has been removed. Scale bar, $1 \text{ } \mu\text{m}$. **f**, Left: schematics of the two consecutive combing steps used to define a crossed nanowire array. The first layer of combed nanowires, produced in the standard manner, is treated as a substrate and processed in the standard manner for nanocombing the second crossed array of nanowires. Note that during the second perpendicular combing process, a thicker resist layer ($\sim 80 \text{ nm}$) was used, and the window was cleaned for 10 s in buffered oxide etch (BOE, 1:7, Transene) and modified with developer (MF-CD-26) before nanocombing. Right: SEM image of a silicon nanowire crossbar array. The resist layer has been removed. Scale bar, $1 \text{ } \mu\text{m}$. The first combing was horizontal (from left to right) and the second combing was vertical (from bottom to top).

predetermined anchoring window pattern and separation determined by the trimming step described already. An SEM image of the devices produced in this manner (Fig. 4b) demonstrates a high yield (70%) of single-nanowire devices, with the remainder being double-nanowire (20%) and open contacts (10%). This lateral position control, at the single-nanowire level, could greatly facilitate an efficient hybrid post-growth assembly (by nanocombing) with top-down fabrication.

Finally, we demonstrate the generality of the nanocombing for (i) assembly and alignment of ultralong nanowires and (ii) creating more complex structures. Alignment of ultralong, millimetre-scale nanowires represents a significant challenge for assembly, but has the potential to enable integration along single nanostructures of many devices and even circuits^{27,28}. Notably, using the same nanocombing procedures described above for ultralong silicon nanowires (Fig. 4c) demonstrates excellent alignment (for example, $>96\%$ aligned within $\pm 1^\circ$) of all the nanowires in the array with an average length of $\sim 140\ \mu\text{m}$, including nanowires as long as $400\ \mu\text{m}$. Indeed, alignment is maintained even at the millimetre scale, as shown in Fig. 4d. Interestingly, this level of alignment in long nanowire structures is comparable to that found in studies describing guided epitaxial nanowire growth along surface step edges²⁹ and guided carbon nanotube growth³⁰, and thus demonstrates our post-growth assembly strategy can obtain complementary levels of control.

The nanocombing technique provides a unique advantage for creating arrays of suspended nanodevices, because the anchoring regions can be registered immediately before pre-etched surface trenches, so that the nanowires are then combed over the trench (Supplementary Fig. S8). For example, nanocombing 50-nm-diameter silicon nanowires over a $1.2\text{-}\mu\text{m}$ -wide and 600-nm-deep trench (Fig. 4e) shows a high yield of well-aligned and straight nanowires suspended over the trench. The density of the suspended nanowires is similar to that observed for nanocombing on flat substrates under the same conditions. This direct assembly of suspended nanowires minimizes the potential detrimental effect of post-placement trench etching^{31,32}, and, moreover, the good alignment and controllable density in the suspended nanowire arrays could facilitate scalable electromechanical devices³³. We have also exploited the well-defined registration of one edge of the nanowire arrays produced by nanocombing to carry out multistep assembly of orthogonal nanowire crossbar arrays, as illustrated schematically in Fig. 4f (left). A representative SEM image of the nanowire array produced by this method demonstrates a well-aligned crossbar structure (Fig. 4f, right). The registration of ends in the two combing steps enables a much higher yield of cross-points (per array) than achieved previously by assembly^{5,9,13}. More generally, we believe these nanocombing studies show clearly the possibility of realizing proposed¹ post-growth bottom-up assembly of distinct nanowire materials into multilayer, three-dimensional, single-nanowire-based nanoelectronics in the future.

Methods

Nanowire synthesis. The silicon and Ge/Si core-shell nanowires were grown by a nanocluster-catalysed vapour-liquid-solid method described previously^{23,25–27}. Briefly, the growth substrate (600 nm SiO_2/Si) was cleaned by oxygen plasma (80 W, 1 min), treated with poly-L-lysine solution (0.1%, Ted Pella) for 5 min, and then rinsed thoroughly with deionized water. Gold nanoparticles (Ted Pella) were then dispersed on the growth substrate at a nanoparticle density of $\sim 30\ \mu\text{m}^{-2}$. Specifically, gold nanoparticles with diameters of 15–20 nm were used for the silicon-nanowire synthesis²³. The growth was carried out at 450°C under a constant pressure of 40 torr, with SiH_4 (2.5 s.c.c.m.), diluted B_2H_6 (100 ppm in He, 3 s.c.c.m.) and H_2 (60 s.c.c.m.) as reactant, doping and carrier gases, respectively. The growth time was ~ 50 min, producing an average length of $\sim 30\ \mu\text{m}$. The ultralong silicon-nanowire synthesis was carried out at 415°C and 10 torr using Si_2H_6 (3 s.c.c.m.) and H_2 (10 s.c.c.m.) as the reactant and carrier gases, respectively²⁷. The growth time was 20 min, producing an average length of $\sim 600\ \mu\text{m}$. Gold nanoparticles with diameters of 10 nm were used for the Ge/Si core-shell nanowire synthesis^{25,26}. The germanium-core nanowire was grown at 270°C and 450 torr, with GeH_4

(30 s.c.c.m., 10% in H_2) and H_2 (200 s.c.c.m.) as the reactant and carrier gases, respectively. The growth time was 50 min, producing an average length $\sim 30\ \mu\text{m}$. Without opening the growth system, the epitaxial silicon shell was then grown at 460°C and 5 torr for 2 min using SiH_4 (5 s.c.c.m.) as the reactant gases.

Resist-based nanocombing. Resist (Microposit S1805, 1:3 (vol:vol) diluted in Microposit Thinner-P) at a thickness of ~ 70 nm was spin-coated on the target substrate. During the photolithography process for the anchoring-window definition, a development time of 50 s (Microposit MF-CD-26 or MF-319) was used, followed by a short deionized-water rinse (10 s) and nitrogen drying. The target substrate was then mounted onto a movable stage controlled by a micromanipulator¹⁸. Approximately $40\ \mu\text{l}$ oil (heavy mineral oil, viscosity $\nu \approx 70\ \text{mPa s}$, #330760, Sigma-Aldrich) was drop-cast onto the target substrate as the lubricant. The growth substrate ($\sim 1.2\ \text{cm} \times 1.2\ \text{cm}$) was then brought into contact with the target substrate with a constant pressure of $\sim 4.8\ \text{N cm}^{-2}$. During combing, the target substrate was moved by the micromanipulator at a constant velocity of $\sim 5\ \text{mm min}^{-1}$ with respect to the fixed growth substrate. Because the tetramethylammonium hydroxide contained in the developer also serves to modify the SiO_2 surface and thereby improve nanowire anchoring, a development time of >20 s was necessary. Finally, the developed substrate was rinsed briefly with deionized water (10 s) immediately before the start of the combing process. For the ultralong silicon nanowires, a reduced deionized-water washing time (3 s) was used to increase anchoring efficiency. The above procedure can be readily applied to different target substrates such as silicon nitride (Si_3N_4) and sapphire (Al_2O_3) using the same or different resist (SU-8, Microchem). Following nanocombing transfer, the oil and resist layer were removed as described in Supplementary Fig. S7. For electron-beam lithography-based nanocombing, poly(methyl methacrylate) (PMMA, 950-C2, Microchem, 50 nm thick) was used as the combing surface. The exposed SiO_2/Si (anchoring) surface was treated in MF-319 developer for 50 s, and then rinsed in deionized water for $\sim 15\text{--}30$ s. The same combing process as introduced above was then used.

Suspended nanowires. Trenches were fabricated using electron-beam lithography by defining open stripes with widths of $1\text{--}2\ \mu\text{m}$ on the target substrate (600 nm SiO_2/Si). The developed resist layer (methyl methacrylate (MMA) + PMMA 950-C5, Microchem) was used as the sacrificial mask for reactive ion etching of SiO_2 in the open stripes, with a typical trench depth of ~ 600 nm. Following removal of the resist layer in acetone, the procedure described above was used to define anchoring windows, transfer silicon nanowires by nanocombing, and remove the oil and resist layer. Silicon nanowires with an average diameter of 50 nm and average length of $\sim 30\ \mu\text{m}$ were used.

Nanocombed nanowire statistics. The statistics are based on 1,643 nanowires from the same sample in Fig. 1 with the angle distribution shown in Fig. 1e. Specifically, 1,620 of the 1,643 ($\sim 98.6\%$) of the nanowires were aligned within $\pm 1^\circ$ of the combing direction. By the definition of alignment used in other reports (within $\pm 5^\circ$ of the average direction)^{12,13}, this produces an alignment rate of $\sim 99.6\%$ (1,637 out of 1,643), or a misalignment rate of $\sim 0.4\%$, which is over one order of magnitude lower than reported values^{5,12–14}. The number of defects, defined as the crossing between nanowires, is 28 or ~ 0.04 nanowire per μm , which is over one order of magnitude lower than reported values¹⁸.

Received 27 July 2012; accepted 12 March 2013;
published online 21 April 2013

References

- Lu, W. & Lieber, C. M. Nanoelectronics from the bottom up. *Nature Mater.* **6**, 841–850 (2007).
- Wang, M. C. P. & Gates, B. D. Directed assembly of nanowires. *Mater. Today* **12**, 34–43 (May, 2009).
- Smith, P. A. *et al.* Electric-field assisted assembly and alignment of metallic nanowires. *Appl. Phys. Lett.* **77**, 1399–1401 (2000).
- Duan, X., Huang, Y., Cui, Y., Wang, J. & Lieber, C. M. Indium phosphide nanowires as building blocks for nanoscale electronic and optoelectronic devices. *Nature* **409**, 66–69 (2001).
- Huang, Y., Duan, X., Wei, Q. & Lieber, C. M. Directed assembly of one-dimensional nanostructures into functional networks. *Science* **291**, 630–633 (2001).
- Duan, X. *et al.* High-performance thin-film transistors using semiconductor nanowires and nanoribbons. *Nature* **425**, 274–278 (2003).
- Hangerter, C. M. & Myung, N. V. Magnetic alignment of nanowires. *Chem. Mater.* **17**, 1320–1324 (2005).
- Tao, A. *et al.* Langmuir–Blodgett silver nanowire monolayers for molecular sensing using surface-enhanced Raman spectroscopy. *Nano Lett.* **3**, 1229–1233 (2003).
- Whang, D., Jin, S., Wu, Y. & Lieber, C. M. Large-scale hierarchical organization of nanowire arrays for integrated nanosystems. *Nano Lett.* **3**, 1255–1259 (2003).
- Jin, S. *et al.* Scalable interconnection and integration of nanowire devices without registration. *Nano Lett.* **4**, 915–919 (2004).

11. Javey, A., Nam, S., Friedman, R. S., Yan, H. & Lieber, C. M. Layer-by-layer assembly of nanowires for three-dimensional, multifunctional electronics. *Nano Lett.* **7**, 773–777 (2007).
12. Yerushalmi, R., Jacobson, Z. A., Ho, J. C., Fan, Z. & Javey, A. Large scale, highly ordered assembly of nanowire parallel arrays by differential roll printing. *Appl. Phys. Lett.* **91**, 203104 (2007).
13. Fan, Z. *et al.* Wafer-scale assembly of highly ordered semiconductor nanowire arrays by contact printing. *Nano Lett.* **8**, 20–25 (2008).
14. Yu, G., Cao, A. & Lieber, C. M. Large-area blown bubble films of aligned nanowires and carbon nanotubes. *Nature Nanotech.* **2**, 372–377 (2007).
15. Li, M. *et al.* Bottom-up assembly of large-area nanowire resonator arrays. *Nature Nanotech.* **3**, 88–92 (2008).
16. Fan, Z. *et al.* Toward the development of printable nanowire electronics and sensors. *Adv. Mater.* **21**, 3730–3743 (2009).
17. Freer, E. M., Grachev, O., Duan, X., Martin, S. & Stumbo, D. P. High-yield self-limiting single-nanowire assembly with dielectrophoresis. *Nature Nanotech.* **5**, 525–530 (2010).
18. Nam, S.-W. *Assembly and Integration of Nanowires and Graphene for Nanoelectronics and Nanobiotechnology* Ch. 2 (Harvard Univ. Press, 2011).
19. Ishikawa, F. N. *et al.* Transparent electronics based on transfer printed aligned carbon nanotubes on rigid and flexible substrates. *ACS Nano* **3**, 73–79 (2009).
20. Takei, K. *et al.* Nanowire active-matrix circuitry for low-voltage macroscale artificial skin. *Nature Mater.* **9**, 821–826 (2010).
21. Cao, Q. *et al.* Medium-scale carbon nanotube thin-film integrated circuits on flexible plastic substrates. *Nature* **454**, 495–500 (2008).
22. Michalet, X. *et al.* Dynamic molecular combing: stretching the whole human genome for high-resolution studies. *Science* **277**, 1518–1523 (1997).
23. Cui, Y., Zhong, Z., Wang, D., Wang, W. U. & Lieber, C. M. High performance silicon nanowire field effect transistors. *Nano Lett.* **3**, 149–152 (2003).
24. Cai, L., Bahr, J. L., Yao, Y. & Tour, J. M. Ozonation of single-walled carbon nanotubes and their assemblies on rigid self-assembled monolayers. *Chem. Mater.* **14**, 4235–4241 (2002).
25. Yan, H. *et al.* Programmable nanowire circuits for nanoprocessors. *Nature* **470**, 240–244 (2011).
26. Xiang, J., Lu, W., Hu, Y., Yan, H. & Lieber, C. M. Ge/Si nanowire heterostructures as high-performance field-effect transistors. *Nature* **441**, 489–493 (2006).
27. Park, W. I., Zheng, G., Jiang, X., Tian, B. & Lieber, C. M. Controlled synthesis of millimeter-long silicon nanowires with uniform electronic properties. *Nano Lett.* **8**, 3004–3009 (2008).
28. Yaman, M. *et al.* Arrays of indefinitely long uniform nanowires and nanotubes. *Nature Mater.* **10**, 494–501 (2011).
29. Tsivion, D., Schwartzman, M., Popovitz-Biro, R., von Huth, P. & Joselevich, E. Guided growth of millimeter-long horizontal nanowires with controlled orientations. *Science* **333**, 1003–1007 (2011).
30. Kang, S. J. *et al.* High-performance electronics using dense, perfectly aligned arrays of single-walled carbon nanotubes. *Nature Nanotech.* **2**, 230–236 (2007).
31. Husain, A. *et al.* Nanowire-based very-high-frequency electromechanical resonator. *Appl. Phys. Lett.* **83**, 1240–1242 (2003).
32. Sazonova, V. *et al.* A tunable carbon nanotube electromechanical oscillator. *Nature* **431**, 284–287 (2004).
33. Feng, X. L., He, R., Yang, P. & Roukes, M. L. Very high frequency silicon nanowire electromechanical resonators. *Nano Lett.* **7**, 1953–1959 (2007).

Acknowledgements

The authors thank J. Ellenbogen, S. Das and J. Klemic for helpful discussion, and J. Huang for modification of the nanocombing assembly tool. C.M.L. acknowledges support of this work from a contract from the MITRE Corporation (awards 92007 and 92009) and a National Security Science and Engineering Faculty Fellow award (N00244-09-1-0078).

Author contributions

J.Y. and C.M.L. designed the experiments. J.Y. performed the experiments and data analysis. H.Y. helped in nanowire synthesis and device fabrication. J.Y. and C.M.L. co-wrote the manuscript. All authors discussed the results and commented on the manuscript.

Additional information

Supplementary information is available in the [online version](#) of the paper. Reprints and permissions information is available online at www.nature.com/reprints. Correspondence and requests for materials should be addressed to C.M.L.

Competing financial interests

The authors declare no competing financial interests.